

Modeling of Holey Fiber Tapers With Selective Transmission for Sensor Applications

Vladimir P. Minkovich, *Member, IEEE*, David Monzón-Hernández, *Member, IEEE*,
Joel Villatoro, *Member, IEEE*, Alexander B. Sotsky, and Luidmila I. Sotskaya

Abstract—The theoretical modeling of large-mode-area silica holey fiber tapers with collapsed air holes that are fabricated with a nonadiabatic process is reported. The transmission spectra of such tapers exhibit multiple interference peaks due to the beating between two modes of the taper waist. The devices investigated here can be useful for a variety of sensor applications since the interference peaks are sensitive to the external environment. Our theoretical model confirms the experimental results.

Index Terms—Holey fiber (HF), interferometry, optical fiber devices, optical fiber interferometer, optical fiber sensors.

I. INTRODUCTION

THE UNUSUAL guiding mechanism and the structure of photonic-crystal fibers [1], [2], also known as microstructured fibers or holey fibers (HFs), offer new possibilities for the development of optical sensors. Such possibilities are being investigated in different laboratories around the world. HFs provide an efficient method to exploit the interaction of the guided light with different gases, liquids, or biological samples present inside the holes [3]–[6]. The advantage of this alternative is that the HF itself can work as a chamber. In addition, some parameters such as the size of the holes and the separation between the holes can be optimized to improve the overlap between the parameter being sensed and the mode field [7]. HFs combined with tapering technology also offer new possibilities for optical sensing [8], [9]. In this case, one can either taper the HF and preserve its structure [8] or taper the fiber and collapse the air holes over a localized region [9]. In both cases, the tapering is adiabatic, and it makes the HF to become sensitive to the external environment. Although the tapers reported in [8] and [9] are suitable for evanescent wave sensing, no sensors based on them have been demonstrated yet.

HFs can also be tapered with a nonadiabatic process. With such a process, the air holes of the fibers can be gradually

collapsed over a length of several millimeters. The collapsing of the voids transforms a section of an HF into a piece of solid multimode fiber. This transformation allows the coupling and beating between the guided modes and makes the transmission spectrum of the tapers to exhibit an oscillatory pattern. In a previous publication, we reported some preliminary results on the application of a tapered HF with collapsed air holes for refractive-index sensing [10]. Our findings reported in [10] the need for a complete explanation of the origin of the interference peaks, and the potential applications of HF tapers with collapsed air holes for different sensing purposes served as a motivation for this paper. We provide here a detailed theoretical investigation of the transmission properties of a tapered large-mode-area HF with collapsed air holes. Some experimental results are also provided to corroborate the theoretical calculations. The results presented here may be useful for the design of novel sensors based on nonadiabatically tapered HFs.

II. MODAL PROPERTIES OF TAPERED HFS

The fiber employed in our experiments was fabricated in our facilities. It was a large-mode-area HF with solid core surrounded by a few air holes in the cladding. The fabrication and properties of such a fiber are described in detail in [11] and [12]. A cross section of the cleaved end of our HF and a schematic representation of the taper are shown in Fig. 1. The diameter of the solid core is 11 μm , the average hole diameter d is 2.73 μm , and the average hole spacing, or pitch, Λ is 5.45 μm . As one can see in Fig. 1(a), the HF consists of four full rings of air holes arranged in a hexagonal pattern (the fifth ring is partially collapsed). Before the tapering, the HF was spliced to a standard single-mode fiber in order to seal the ends. The length of the HF was approximately 30 cm, although a shorter length can also be employed. Then, we stretched the HF while it was being heated with an oscillating high-temperature flame torch. All the tapering conditions are described in detail elsewhere [13]. The length of oscillation of the torch, and also the length of the uniform waist of the taper, was in the 3–5-mm range. We fabricated several samples with waist diameters between 10 and 80 μm .

To analyze the transmission spectra of the tapers, we implemented a simple light transmission measurement setup consisting of a low-power light-emitting diode (LED), with peak emission at 1280 and 80 nm of spectral width and a high-resolution optical spectrum analyzer. The measured transmission spectra of three tapered HFs and also the radiation spectrum of the LED are shown in Fig. 2. The waist diameters

Manuscript received April 11, 2006; revised August 3, 2006. This work was supported by the Consejo Nacional de Ciencia y Tecnología, Mexico, under Grants 42986-F and P 46972-F and by the Consejo Estatal de Ciencia y Tecnología de Guanajuato, Mexico, under Grant 0504K117026. The work of J. Villatoro was supported by the Ministerio de Educación y Ciencia, Spain, under the “Ramón y Cajal” program.

V. P. Minkovich and D. Monzón-Hernández are with the Centro de Investigaciones en Óptica, A.C., Leon 37150, Mexico (e-mail: vladimir@cio.mx; dmonzon@cio.mx).

J. Villatoro is with the Nanophotonics Group, Institute of Photonic Sciences (ICFO), 08860 Castelldefels, Barcelona, Spain (e-mail: joel.villatoro@icfo.es).

A. B. Sotsky is with the Mogilev State University, Mogilev 212000, Belarus.

L. I. Sotskaya is with the Mogilev State Foodstuffs University, Mogilev 212030, Belarus.

Digital Object Identifier 10.1109/JLT.2006.884207

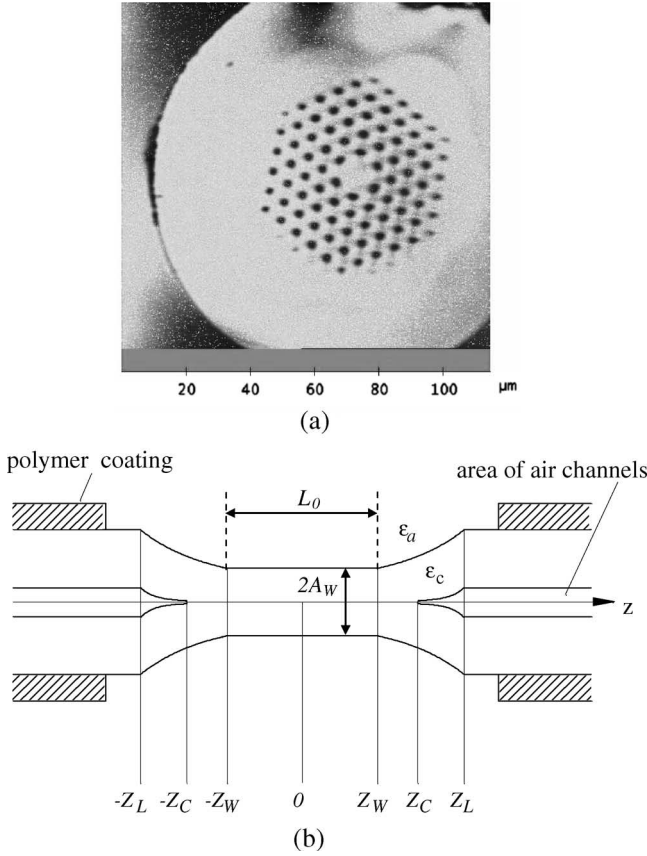


Fig. 1. (a) Image of the cross section of an untapered HF used in our experiments. The outer diameter of the HF is 125 μm , and the relative hole diameter $d/\Lambda = 0.5$. (b) Illustration of a uniform-waist tapered HF. L_0 and A_w are the length and the radius of the taper waist, respectively. The variables that appear in the figure are discussed in the text.

of the tapers, from top to bottom of Fig. 2(a) were 44, 32.6, and 15 μm , respectively. All the spectra were normalized with respect to the maxima of the highest peak. We can note from the figure that the spectrum of the 44- μm -thick taper is basically the output spectrum of the LED. However, the spectra of the tapers with waist diameters of 32.6 and 15 μm exhibit a series of peaks. In Fig. 2(a), we can see that the number of peaks increases as the diameter of the taper is reduced. Note also that the peaks become sharper as the taper becomes thinner. It is important to point out that the nonadiabatic tapering of our HF introduces losses, but they are typically below 3 dB.

To understand the origin of the peaks shown in Fig. 2(a), we analyzed the optical field in a tapered large-mode-area HF by the beam propagation method. For the calculations, we considered that the rays of light in a real taper make small angles with silica-air interfaces.

In this case, the following scalar approximation for the lateral components $u(\rho, \varphi, z)$ of the optical field can be applied [14]–[16]:

$$\frac{\partial^2 u}{\partial \rho^2} + \frac{1}{\rho} \frac{\partial u}{\partial \rho} + \frac{1}{\rho^2} \frac{\partial^2 u}{\partial \varphi^2} + \frac{\partial^2 u}{\partial z^2} + k_0^2 (\epsilon_s + \Delta \epsilon) u = 0 \quad (1)$$

$$u|_{\rho=A(z)} = 0. \quad (2)$$

Here, ρ , φ , and z are the cylindrical coordinates, $k_0 = 2\pi/\lambda_0$ is the wavenumber of free space, $\Delta \epsilon = \epsilon(\rho, \varphi, z) - \epsilon_s$, in which

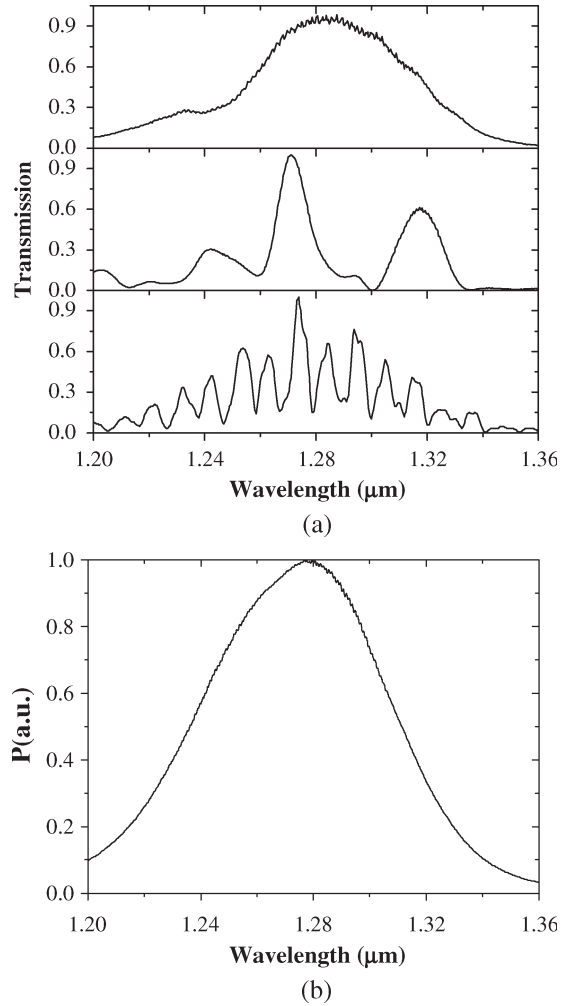


Fig. 2. (a) Transmission spectra of three tapered HFs with waist diameters of 44 μm (top plot), 32.6 μm , and 15 μm (bottom plot). (b) Radiation spectrum of the LED used.

$\epsilon(\rho, \varphi, z)$ is the permittivity of the medium inside the taper, including the air channels, and ϵ_s is the permittivity of the silica glass. $A(z)$ is a local outer radius of the taper [see Fig. 1(b)]. The function $u(\rho, \varphi, z)$ can be expressed in the form of an expansion of local modes of a uniform fiber of radius $A(z)$ given as follows:

$$u(\rho, \varphi, z) = \exp(-ikz) \sum_{\nu=-m}^m \sum_{s=1}^{n(\nu)} C_{\nu s}(z) u_{\nu s}(\rho, \varphi, z). \quad (3)$$

The term $\exp(-ikz)$ is a phase factor that is included for convenience in later analysis, $k = k_0 \sqrt{\epsilon_s}$, $C_{\nu s}(z)$ are unknown amplitudes, and m and $n(\nu)$ are the reduction orders of the expansion. The base functions $u_{\nu s}(\rho, \varphi, z)$ in (3) have the form

$$u_{\nu s} = \exp(i\nu\varphi) J_\nu(\kappa_{\nu s} r) \quad (4)$$

where $r = \rho/A(z)$, and $\kappa_{\nu s}$ are the zeroes of the Bessel functions [$J_\nu(\kappa_{\nu s}) = 0$]. At $m \rightarrow \infty$ and $n(\nu) \rightarrow \infty$, the functions $u_{\nu s}(\rho, \varphi, z)$ form a full set of functions for two variables ρ and φ at any values of the longitudinal coordinate z [17]. Therefore, a possibility of the notion (3) must give no rise to doubts.

By substituting (3) into (1) and using the Galerkin's procedure, we get the following system of ordinary differential equations with respect to the amplitudes of the local modes:

$$\begin{aligned}
& \frac{d^2 C_{\nu s}}{dz^2} \\
& = 2ik \frac{dC_{\nu s}}{dz} + \frac{1}{A^2} \left[\kappa_{\nu s}^2 - \nu^2 \left(\frac{dA}{dz} \right)^2 \right] C_{\nu s} \\
& + \frac{1}{N_{\nu s}} \sum_{j=1}^{n(\nu)} \left\{ C_{\nu j} \left(\frac{\kappa_{\nu j}}{A} \frac{dA}{dz} \right)^2 I_{\nu s j}^{(3)} \right. \\
& \quad \left. + \left[\frac{dC_{\nu j}}{dz} \frac{\kappa_{\nu j}}{A} \frac{dA}{dz} - C_{\nu j} \frac{\kappa_{\nu j}}{A} \right. \right. \\
& \quad \left. \left. \times \left(\frac{1}{A} \left(\frac{dA}{dz} \right)^2 - \frac{d^2 A}{dz^2} + 2ik \frac{dA}{dz} \right) \right] I_{\nu s j}^{(2)} \right\} \\
& - \frac{k_0^2}{2\pi N_{\nu s}} \sum_{\mu=-m}^m \sum_{l=1}^{n(\mu)} K_{\nu s \mu l} C_{\mu l} \quad (5)
\end{aligned}$$

where

$$N_{\nu s} = \int_0^1 x J_\nu^2(\kappa_{\nu s} x) dx = 0.5 J_{\nu+1}(\kappa_{\nu s})$$

$$I_{\nu s j}^{(2)} = \int_0^1 x J_\nu(\kappa_{\nu s} x) \frac{\partial J_\nu(\kappa_{\nu j} x)}{\partial \kappa_{\nu j}} dx$$

$$I_{\nu s j}^{(3)} = \int_0^1 x^3 J_\nu(\kappa_{\nu s} x) J_\nu(\kappa_{\nu j} x) dx$$

$$K_{\nu s \mu l} = \int_0^1 x J_\nu(\kappa_{\nu s} x) M_{\mu-\nu}(\rho, z) J_\mu(\kappa_{\mu l} x) dx$$

$$M_\alpha(\rho, z) = \int_0^{2\pi} \Delta \varepsilon \exp(i\alpha\varphi) d\varphi.$$

Note that (5) is written in an approximation of the zero boundary condition given in (2). However, for sensing applications, it is important to include the influence of the external medium on the optical field in the taper. This can be done, in the first order of the perturbation theory, by replacing $\kappa_{\nu s}$ by $\bar{\kappa}_{\nu s}$ in (5), where $\bar{\kappa}_{\nu s}$ is expressed as [15]

$$\bar{\kappa}_{\nu s} = \kappa_{\nu s} \sqrt{1 - (\varepsilon_s + \varepsilon_a)(k_0 A \sqrt{\varepsilon_s - \varepsilon_a})^{-2}}. \quad (6)$$

To the left ($z < -Z_L$) as well as to the right ($z > Z_L$) of the tapered zone [see Fig. 1(b)], we have untapered HF, both with constant radii $A(z) = A_0$. Since $k_0 A_0 \gg 1$, the HF's can support a multitude of eigenmodes. The fields of these modes

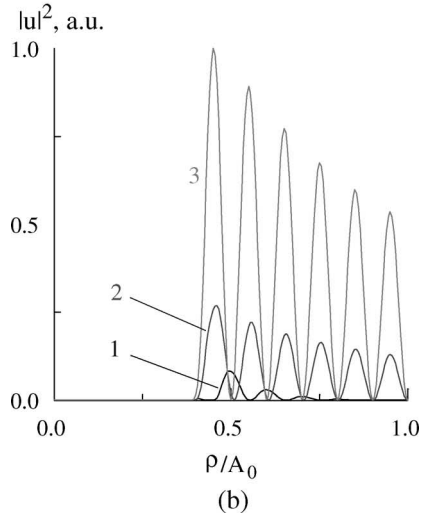
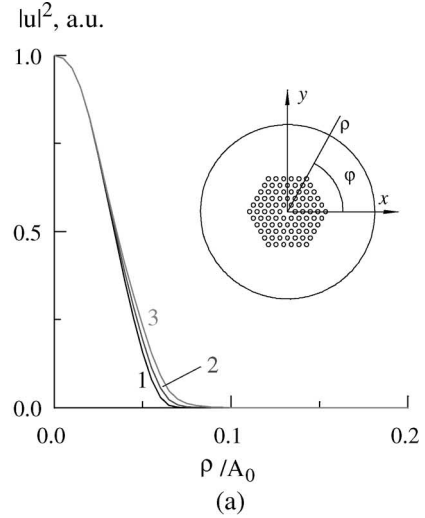


Fig. 3. (a) Intensity distributions of the HF fundamental mode and (b) the first higher order mode of the HF, for which modulus $|\beta_l - \beta_0|$ ($l > 0$) is minimal at $\lambda_0 = 1.31 \mu\text{m}$. In both figures, curves 1, 2, and 3 correspond to $\varphi = 0$, $\varphi = \pi/4$, and $\varphi = \pi/2$, respectively. The inset illustrates the cross section of the HF.

are described by the expression (3), in which the amplitudes $C_{\nu s}(z)$ are replaced by $C_{\nu s}^{(l)}(z)$, where

$$C_{\nu s}^{(l)}(z) = G_l \exp[i(k - \beta_l)z] a_{\nu s}^{(l)} N_{\nu s}^{-0.5} \quad (7)$$

where $l \geq 0$ is the mode number ($l = 0$ refers to the fundamental mode), G_l is the amplitude of the mode, β_l is the mode propagation constant, and the $a_{\nu s}^{(l)}$ are unknown coefficients. The values of $a_{\nu s}^{(l)}$ and β_l can be found by solving the following algebraic eigenvalue problem:

$$(k^2 - \beta_l^2 - \kappa_{\nu s}^2 A_0^{-2}) a_{\nu s}^{(l)} + \frac{k_0^2}{2\pi} \sum_{\mu=-m}^m \sum_{j=1}^{n(\mu)} \frac{K_{\nu s \mu j}}{\sqrt{N_{\nu s} N_{\mu j}}} a_{\mu j}^{(l)} = 0. \quad (8)$$

Equation (8) follows from the differential equation (5) with the assumption that $dA/dz \equiv 0$.

The distributions of the mode fields for an untapered HF are shown in Figs. 3 and 4. The fields were computed by assuming

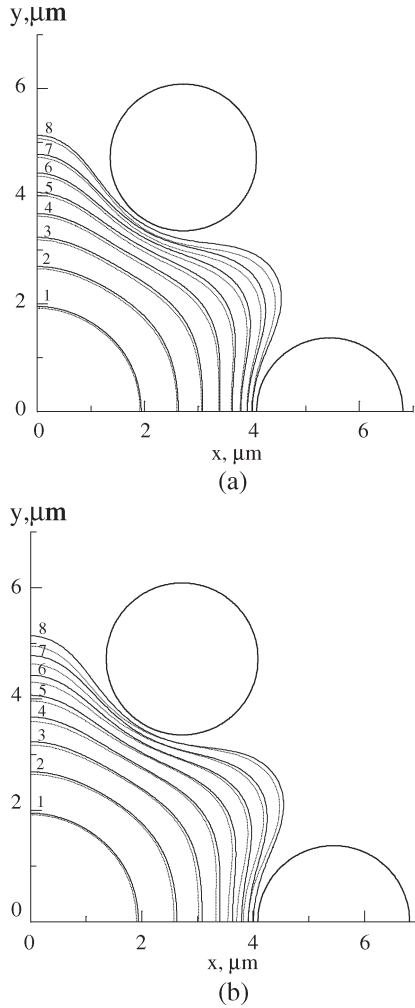


Fig. 4. One-quarter parts of the intensity distributions for the HF fundamental modes with the main components of the magnetic field (a) H_x and (b) H_y . Isolines 1, 2, 3, . . . , 8 of the normalized longitudinal component $S_z(\rho, \varphi)$ of the Poynting vector refer to $\ln[S_{z \max}/S_z(\rho, \varphi)] = 0.5, 1, 1.5, \dots, 4$, respectively. Dashed curves are exact results obtained by the method of integral equations; solid curves indicate the scalar approximation.

$N_c = 5$, $a_0 = 1.365 \mu\text{m}$, $A_0 = 62.5 \mu\text{m}$, $\lambda_0 = 1.31 \mu\text{m}$, and $\Lambda_0 = 5.45 \mu\text{m}$, where N_c is the number of hexagonal rings of air holes around the HF core, a_0 is the average air-hole radius, A_0 is the outer radius of the untapered HF, and Λ_0 is the hole spacing or pitch. The value of ε_s was calculated, taking into account Sellmeier’s coefficients of silica. These values correspond to the parameters of the large-mode-area HF with which we fabricated the tapers [see Fig. 1(a)].

The hexagonal symmetry of the HF cross section was taken into account to reduce the computation time. As a result of such symmetry, the following relations are valid:

$$M_\alpha = M_{-\alpha} \tag{9}$$

$$M_{p+6q} = 0 \tag{10}$$

where $p = 1, 2, 3, 4, 5$ and $q = 0, 1, 2, \dots$. Since the coefficients $M_\alpha(\rho, z)$ are different from zero only at α values that are divisible by 6, then it is possible to substitute μ by $6\bar{\mu}$ and ν by $6\bar{\nu}$ in (5) and (8), where $\bar{\mu}, \bar{\nu} = 0, \pm 1, \dots, \pm \text{Int}(m/6)$.

The numerical data used in the plots of Fig. 3 were obtained by taking $m \geq 18$, $n(0) \geq 37$, and $n(6\bar{\nu}) \geq 7$, where $\bar{\nu} \geq 1$.

Note from Fig. 3 that the field of the HF fundamental mode is localized within the core and the ring of the air holes adjacent to it. In contrast, the fields of the higher order modes are localized basically between the cladding and the external medium. These fields are formed by the reflection of light from the external surface of the fiber at $\rho = A_o$. However, such modes die out fast since the surface of the HF is coated with an absorbing polymer [see Fig. 3(b)]. Therefore, we can suppose that the fundamental mode of the HF is the only mode that excites the taper and that the registered signal at the taper output is proportional only to the power of the fundamental mode.

Fig. 4 illustrates applicability of the scalar approximation (3), (4), (7), and (8) for computation of the analyzed HFs. Here, we compare the exact intensity isolines of fundamental modes computed by the full vectorial method of integral equations [18] with those computed on the basis of the described scalar approximation. Fig. 4(a) and (b) refers to fundamental modes with main components of magnetic fields H_x and H_y , respectively. Despite the same propagation constants of these modes [19], their exact intensity distributions are slightly different. However, the intensity distributions are completely the same in the scalar approximation. Fig. 4 shows that the scalar approximation is quite valid for evaluation computations in spite of large difference in indexes of fused silica and air. The effectiveness of the scalar approximation for the HFs under consideration can be explained by the fact that radiation guided by HFs is mainly localized in silica and reflected from the interfaces at sliding angles. In accordance with the well-known perturbation theory [15], it results to low magnitudes of electromagnetic fields at the interfaces and makes it possible to neglect the terms coupling the orthogonal transversal components of the electromagnetic field [15], [16]. Estimates presented in [16] show an increase in the accuracy of the scalar approximation with decreasing a/Λ , where a is the hole radius along the taper, i.e., at the air filling factor lowering. For the considered tapers, the maximal ratio $a/\Lambda = 0.25$ is realized at the taper ends, where $a = a_0$ (see later discussion). The presented arguments are to give credit to the scalar approximation validity. Note also that this approximation results to satisfactory agreement between the theory and experiments (see later discussion).

Let the fundamental mode of the HF enters the contracting zone of the taper, i.e., from $z < 0$. Then, if one ignores the weak reflection of the radiation from the taper, the initial conditions given in (5) can be expressed as

$$C_{\nu s}(-Z_L) = a_{\nu s}^{(0)} N_{\nu s}^{-0.5}$$

$$\left. \frac{dC_{\nu s}}{dz} \right|_{z=-Z_L} = i(k - \beta_0) C_{\nu s}(-Z_L). \tag{11}$$

A numerical integration of the Cauchy problem given in (5) or (11) (for instance, by the Runge–Kutta method) presents just a few problems. By calculating the amplitudes $C_{\nu s}(Z_L)$ from (5) and (11), one can write the ratio of the power of the

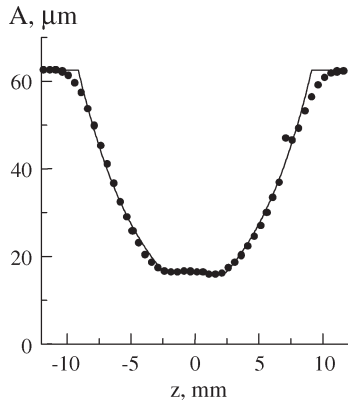


Fig. 5. Profile of the fabricated HF taper with parameters $L_0 = 5$ mm, $Z_w = 2.5$ mm, and $A_w = 16.3$ μm . Solid line represents the theoretical dependence computed by using (12)–(15); points are experimental data.

fundamental HF mode at the output of the taper to the power of this mode at the input of the taper as

$$\eta = \left| \sum_{\nu=0}^m \sum_{s=1}^{n(\nu)} C_{\nu s}(L) a_{\nu s}^{(0)} \sqrt{N_{\nu s}} \right|^2.$$

This formula can be easily deduced using the orthogonality of the functions $u_{\nu s}(\rho, \varphi, z)$ and the normalization [17]

$$\sum_{\nu=-m}^m \sum_{s=1}^{n(\nu)} \left| a_{\nu s}^{(0)} \right|^2 = 1.$$

For numerical modeling of the taper transmission, i.e., for calculating the function $\eta(\lambda_0)$, it is necessary to know the parameters along the HF taper. For this purpose, we used a commercial “Beta LaserMike” gauge to measure the outer diameter in different points along one of our tapers. The experimental data and a fitting line to the data are shown in Fig. 5. The theoretical fitting to the experimental data was done by assuming that the taper diameter varied with z [see Fig. 1(b)] as

$$A(z) = A_0, \quad \text{at } |z| \geq Z_L \quad (12)$$

$$A(z) = A_w = A_0 \exp[(Z_w - Z_L)/L_0], \quad \text{at } |z| \leq Z_w \quad (13)$$

$$A(z) = A_0 \exp[-(z + Z_L)/L_0], \quad \text{at } -Z_L \leq z \leq -Z_w \quad (14)$$

$$A(z) = A_0 \exp[(z - Z_L)/L_0], \quad \text{at } Z_w \leq z \leq Z_L. \quad (15)$$

Note that we assume that the taper waist radius A_w is constant within the interval $-Z_W < z < Z_W$, where $Z_W \approx 0.5L_0$. The function $A(z)$, which is calculated using (12)–(15), is shown in Fig. 5 by a solid line. We took $A_0 = 62.5$ μm , and L_0 was determined by processing the experimental points by the least squares method. Note that the experimental measurements and the theoretical fitting are in good agreement.

Now, if the outer diameter of the HF varies with z , then the separation between the air holes or pitch Λ and the diameter of

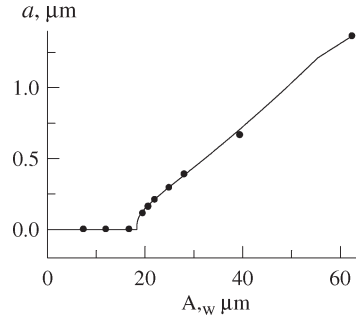


Fig. 6. Dependence of the average air channels radii on the outer radius A_w of the HF taper. Solid curve was computed on a basis of (17)–(19) at $\alpha = 0.35$; points are experimental data.

the holes also vary with z . Before the air holes collapse, we can suppose that the pitch varies with z .

To explore these dependencies, we have performed a microscopic analysis of cross sections of HFs cleaved in the taper waist. Our measurements have shown that in the absence of any collapse of the air holes, the average pitch Λ was approximately proportional to the waist radius A_w . This result is similar to results of [20] and [22]. Therefore, in our theoretical model, we believe that

$$\Lambda(z) = A(z)\Lambda_0/A_0. \quad (16)$$

Measuring the averaged radius a in the cross sections, we found that when radius A_w slightly differed from radius A_0 of the untapered fiber, a was proportional to A_w . Therefore, in the range $A_0 \geq A_w \geq A_s$, we put

$$a = a_0 A_w / A_0 \quad (17)$$

where the value of A_s is defined in the latter part of this section. However, with A_w essential decreasing, the $a(A_w)$ dependency became essentially nonlinear. Analyzing the experimental data, we have found the following empirical formula:

$$a = K A_w [(A_w - A_c)/(\bar{A} - A_c)]^\alpha, \quad \text{at } A_s \geq A_w \geq A_c \quad (18)$$

$$a = 0, \quad \text{at } A_w < A_c \quad (19)$$

where $K = 0.012$, $\bar{A} = 25$ μm , $A_c = \bar{A}(M - 0.78)/(M - 1)$, and $M = (0.51)^{1/\alpha}$ were deduced with the help of experimental data. The expression $A_w = A_c$ represents the radius at which collapse of the air channels occur. The value of A_s is expressed as

$$A_s = [a_0(kA_0)^{-1}]^{1/\alpha} (\bar{A} - A_c) + A_c$$

to satisfy the condition of continuity of the function $a(A_w)$.

The exponent α that appears in (18) depends on the heating temperature and on the stretching velocity of the taper. According to our tapering technology and some experimental studies on the dependence of $a(A_w)$, we found that $0 < \alpha \leq 1$. The experimental and theoretical dependence of the average air-hole radius on the taper radius is shown in Fig. 6. The experimental points were obtained by measuring the taper’s holes diameters with an atomic force microscope. The theoretical fit was done

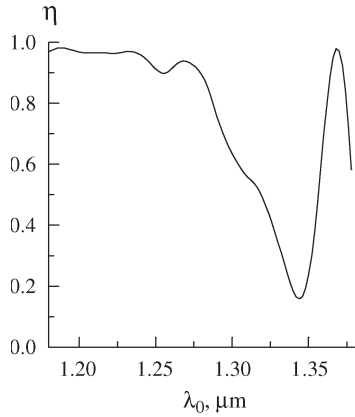


Fig. 7. Computed transmission spectrum of the taper with $A_w = 22 \mu\text{m}$, $L_0 = 5.3 \text{ mm}$, $Z_w = 2.23 \text{ mm}$, and $\alpha = 0.35$.

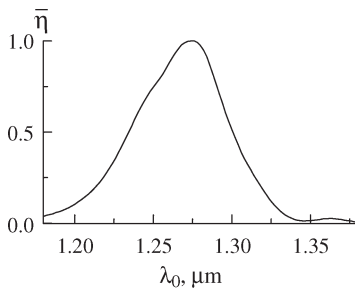


Fig. 8. Computed transmission spectrum of the taper with $A_w = 22 \mu\text{m}$, $L_0 = 5.3 \text{ mm}$, $Z_w = 2.23 \text{ mm}$, and $\alpha = 0.35$ corresponding to excitation of the device by the LED with the radiation spectrum presented in Fig. 2(b).

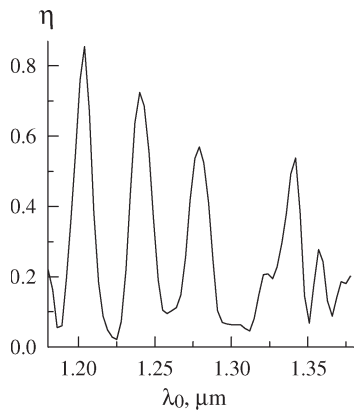


Fig. 9. Computed transmission spectrum of the taper with $A_w = 16.3 \mu\text{m}$, $L_0 = 5 \text{ mm}$, $Z_w = 2.5 \text{ mm}$, and $\alpha = 0.35$.

by applying (17)–(19) after replacing A_w by $A(z)$, where the function $A(z)$ is given in (12)–(15).

III. NUMERICAL DATA, DISCUSSION, AND CONCLUSION

With the theoretical model described earlier, we calculated $\eta(\lambda_0)$ (i.e., the normalized output pattern of the taper) of two tapers with L_0 of about 5 mm but with different waist diameters and one taper with $L_0 = 3 \text{ mm}$. For the same tapers, we also calculated $\bar{\eta}(\lambda_0) = P(\lambda_0)\eta(\lambda_0)$, where $P(\lambda_0)$ is the emission spectrum of the LED employed in the experiments. The results are shown in Figs. 7–12. In all the figures, $1.18 \leq \lambda_0 \leq 1.36 \mu\text{m}$ to match the range of wavelengths of the LED employed.

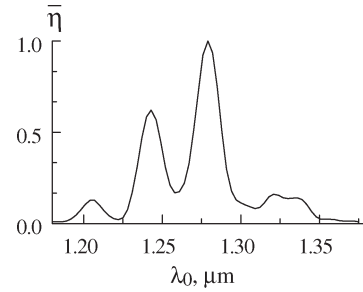


Fig. 10. Computed transmission spectrum of the taper with $A_w = 16.3 \mu\text{m}$, $L_0 = 5 \text{ mm}$, $Z_w = 2.5 \text{ mm}$, and $\alpha = 0.35$ corresponding to excitation of the device by the LED used.

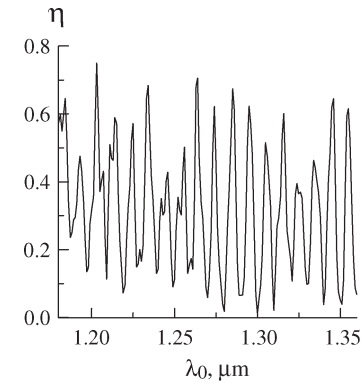


Fig. 11. Computed transmission spectrum of the taper with $A_w = 7.5 \mu\text{m}$, $L_0 = 3 \text{ mm}$, $Z_w = 1.5 \text{ mm}$, and $\alpha = 0.45$.

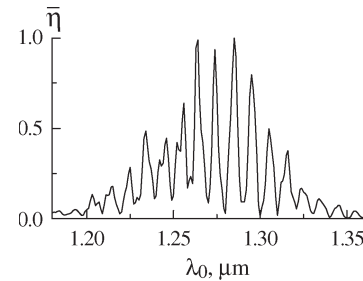


Fig. 12. Computed transmission spectrum of the taper with $A_w = 7.5 \mu\text{m}$, $L_0 = 3 \text{ mm}$, $Z_w = 1.5 \text{ mm}$, and $\alpha = 0.45$ corresponding to excitation of the device by the LED used.

Fig. 7 shows the output pattern of a taper with $A_w = 22 \mu\text{m}$, $L_0 = 5.3 \text{ mm}$, $Z_w = 2.23 \text{ mm}$, and $\alpha = 0.35$. In this taper, the air channels are not collapsed. The average air-hole radius a at the taper waist is equal to $0.21 \mu\text{m}$ (see Fig. 6). The transmission of this taper is close to 100% at $1.18 \mu\text{m} \leq \lambda_0 < 1.3 \mu\text{m}$ (adiabatic regime). However, for $\lambda_0 > 1.3 \mu\text{m}$, the adiabatic condition is broken, and the function $\eta(\lambda_0)$ becomes oscillatory. Note that a similar oscillatory transmission was observed for biconical tapers ($A_w < 5 \mu\text{m}$ and $L_0 < 1 \text{ mm}$) made from conventional single-mode fibers [23]. Fig. 8 shows the output spectrum of the taper, considering that the input light comes from the LED with emission spectrum $P(\lambda_0)$ given in Fig. 2(b). The theoretical spectrum $\bar{\eta}(\lambda_0) = P(\lambda_0)\eta(\lambda_0)$ is in good agreement with the experimental one [compare the top plot of Fig. 2(a) with Fig. 8].

Figs. 9 and 10 show, respectively, the theoretical functions $\eta(\lambda_0)$ and $\bar{\eta}(\lambda_0)$ for a taper with $A_w = 16.3 \mu\text{m}$, $L_0 = 5 \text{ mm}$,

$Z_w = 2.5$ mm, and $\alpha = 0.35$. In this taper, the air channels no longer exist since the collapsing takes place at $A = A_c = 18.3$ μm (see Fig. 6). Such a value of A , according to our theoretical model [see (12)–(15)], indicates that the air channels are collapsed in the region $z = \pm Z_C$, where $Z_C = 3.08$ mm. As a result, at -3.08 mm $< z < 3.08$ mm, we have a piece of multimode optical fiber with variable radius. The modes supported by such a fiber are excited by the HF fundamental mode. The oscillatory behavior of $\eta(\lambda_0)$ (see Fig. 9) is a consequence of the interference between the modes of the piece of solid fiber.

Note that at 1.25 $\mu\text{m} < \lambda_0 < 1.36$ μm , the calculated $\bar{\eta}(\lambda_0)$ of the taper described in Fig. 10 is in good agreement with the experimental transmission spectrum shown in Fig. 2(a). However, outside this wavelength range, the agreement between theory and experiment is not good enough. We believe that the discrepancy is due to the approximate character of the model given in (17)–(19). In real tapers, the radii of the air holes are not exactly identical as we suppose in this model.

The theoretical $\eta(\lambda_0)$ and $\bar{\eta}(\lambda_0)$ of a taper with $A_w = 7.5$ μm , $L_0 = 3$ mm, $Z_w = 1.5$ mm, and $\alpha = 0.45$ ($A_c = 17.9$ μm) are shown in Figs. 11 and 12, respectively. Note that the transmission spectrum for this taper has a pronounced periodicity (the averaged period $\Delta\lambda_0 \cong 0.01$ μm). The same period is observed in the experimental transmission spectrum of the taper with the same parameters [compare the bottom plot of Fig. 2(a) with Fig. 12]. The period of the taper transmission spectra is of interest for sensing applications [10], [23]. Thus, it is important to find a simple expression that gives us such a period.

First, let us consider the system of differential equations that appear in (5) in the half-space $z < 0$ [see Fig. 1(b)]. Let us change the variable z by $-z$ and take the complex conjugate, assuming that ε_s is real. Since $z = 0$ is the plain of symmetry, and taking into account (9) and (10), with the changes, we, again, get the same system of equations of (5). In this case, it is not difficult to conclude that under the condition

$$C_{\nu s}^*(0) = C_{\nu s}(0) \exp(i\phi) \quad (20)$$

where the asterisk denotes the complex conjugate, $\nu = 0, \pm 1, \dots$, $s = 1, 2, \dots$, and ϕ is a constant, the optical field at the output of the taper is identical to the one at the input of the taper. In such a case, the transmittance of the taper has a maximum $\eta = 1$ (ignoring the absorption and reflection effects in the taper). Thus, according to (3), the relations (20) are equivalent to the equality

$$u^*(\rho, \varphi, 0) = u(\rho, \varphi, 0) \exp(i\phi). \quad (21)$$

This equation means that the plain $z = 0$ coincides with the surface of the constant phase of the optical field.

It is obvious that (20) and (21) are approximately valid only for adiabatic tapers in which solely the transmission of the HF fundamental mode takes place [20]. However, the situation changes when the air channels are collapsed. In such a case, we have a piece of an unclad multimode silica fiber in the interval $|z| < Z_C$ [see Fig. 1(b)]. The optical field at the plane $z = 0$ is the result of the interference of all the modes $u_{\nu s}$ supported

by the multimode fiber. Such modes have different propagation constants. If many of modes $u_{\nu s}$ had comparable power, then the phase of the optical field in the plane $z = 0$ would be a fast varying function of the transversal coordinates ρ and φ . In such a case, one can expect the dependence $\eta(\lambda_0)$ to be almost stochastic. However, if the taper has some selective properties, i.e., if it concentrates the light power predominantly in two local modes, let us say in the modes $u_{\nu s}$ and $u_{\mu l}$, then the dependence $\eta(\lambda_0)$ may be periodic.

Let us suppose that the power of the optical field in the region $-Z_C < z < 0$ [see Fig. 1(b)] is concentrated predominantly in the modes $u_{\nu s}$ and $u_{\mu l}$. Thus, the relations for the maximum transmittance of the taper (20) can be applied only to these two modes. If we assume that the phase front of the optical field generated by the HF mode at $z = -Z_C$ is plane, i.e., that the equality

$$C_{\nu s}^*(-Z_C)/C_{\nu s}(-Z_C) = C_{\mu l}^*(-Z_C)/C_{\mu l}(-Z_C)$$

is satisfied, then (20) can be reduced to one equation, i.e.,

$$\int_{-Z_C}^{-Z_W} [\beta_{\nu s}(z) - \beta_{\mu l}(z)] dz + [\beta_{\nu s}(-Z_W) - \beta_{\mu l}(-Z_W)] Z_W = n\pi. \quad (22)$$

In (22), $\beta_{\nu s}(z)$ and $\beta_{\mu l}(z)$ are, respectively, the propagation constants of the local modes $u_{\nu s}$ and $u_{\mu l}$, and n is any integer. Note that (22) means that the difference between the phases of the modes $u_{\nu s}$ and $u_{\mu l}$ after they propagate from $-Z_C$ to Z_C , i.e., the solid section of the taper, is multiple of 2π .

To find a solution of (22), we use the following approximation:

$$\begin{aligned} \beta_{\nu s}(z) &= k_0 \sqrt{\varepsilon_s - \bar{\kappa}_{\nu s}^2 [k_0 A(z)]^{-1}} \\ &\cong k_0 \sqrt{\varepsilon_s} - \frac{\kappa_{\nu s}^2}{2k_0 \sqrt{\varepsilon_s} A^2(z)} \end{aligned} \quad (23)$$

which is valid when $k_0 A(z) \gg 1$ [15].

Substituting (23) into (22) by taking into account (13) and (14) and performing an elementary integration, we get

$$\lambda_0 = n\Delta\lambda_0 \quad (24)$$

where

$$\Delta\lambda_0 = \frac{4\pi^2 \sqrt{\varepsilon_s}}{\left(\kappa_{\mu l}^2 - \kappa_{\nu s}^2 \right) \left[L_0 / (2A_W^2) + Z_W / A_W^2 - L_0 / (2A_C^2) \right]}. \quad (25)$$

Therefore, the transmittance of the taper exhibits maxima only at wavelengths determined by (24) and (25). If one neglects the dispersion of silica, then the taper transmission will be periodic with period $\Delta\lambda_0$ given in (25).

To verify numerically this qualitative reasoning, we computed the dependencies of $P_{\nu s}(z)$, where $P_{\nu s}$ is the ratio of the $u_{\nu s}$ local mode power to the full power of the HF fundamental

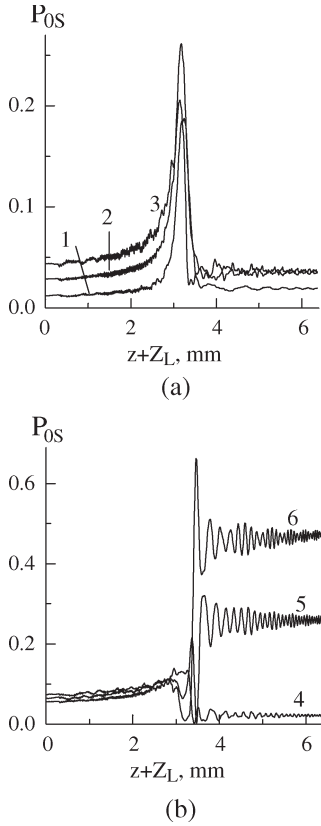


Fig. 13. Computed power distributions for local modes u_{0s} for the section of narrowing of the taper with $A_w = 7.5 \mu\text{m}$, $A_c = 17.9 \mu\text{m}$, $L_0 = 3 \text{ mm}$, and $Z_w = 1.5 \text{ mm}$. The numbers of the curves coincide with the meaning of s at the designation of the mode.

mode at the input of the taper. To do so, we used the following expression:

$$P_{\nu s}(z) = [A(z)/A_0]^2 |C_{\nu s}(z)|^2 N_{\nu s} \quad (26)$$

which results from the orthogonality conditions of the functions $u_{\nu s}(\rho, \varphi)$ [17].

The theoretical functions $P_{\nu s}(z)$ for six modes calculated with (26) for a taper with $A_w = 7.5 \mu\text{m}$, $A_c = 17.9 \mu\text{m}$, $L_0 = 3 \text{ mm}$, and $Z_w = 1.5 \text{ mm}$ are presented in Fig. 13(a) and (b). According to the figure, the HF fundamental mode at the input of the taper ($z = -Z_L$) consists of a wide spectrum of local modes of the uniform fiber. However, as the air channels are narrowed, the optical power is concentrated predominantly in the local modes u_{05} and u_{06} . After the collapse of the air channels at $z > -Z_C$, where $Z_C = 4.22 \text{ mm}$, the exchange of power between the local modes becomes insignificant. It is important to point out that the sum of powers for the modes u_{05} and u_{06} , i.e., $P_\sigma = P_{05}(-Z_W) + P_{06}(-Z_W)$, at the input of the taper waist is more than 70% of the total optical power. It is also necessary to mention that the concentration of optical power in the local modes u_{05} and u_{06} takes place in all the considered range of wavelengths. Fig. 14 shows the dependence of $P_\sigma(\lambda_0)$ for two tapers with different diameters.

Now, let us calculate $\Delta\lambda_0$ with (24) and (25) for the taper described in the previous paragraph. By substituting $\kappa_{05} = 14.93$ and $\kappa_{06} = 18.07$ in (25) [21], we get $\Delta\lambda_0 = 0.011 \mu\text{m}$.

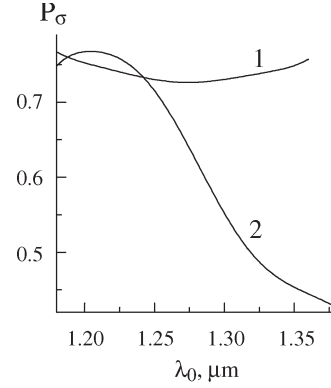


Fig. 14. Total power of the local modes u_{05} and u_{06} at the entrance of the waist for the tapers with $A_w = 7.5 \mu\text{m}$ (curve 1) and $A_w = 16.3 \mu\text{m}$ (curve 2).

Such a value is in good agreement with the theoretical and experimental values given earlier, which confirm the correctness of (25). For comparison, it is necessary to note that the oscillatory transmission spectra of tapers made from conventional single-mode fibers is explained by interference between the fundamental u_{01} mode and the higher order u_{02} mode [23]. For such tapers, $\kappa_{01} = 2.405$ for the fundamental mode and $\kappa_{02} = 5.52$ for the higher order mode [23]. Thus, the period of the interference fringes in abrupt tapers, which is computed by (25), is $\Delta\lambda_0 = 0.048 \mu\text{m}$. This means that the interference fringes of HF tapers are closer in wavelength separation than those of the tapers made from conventional optical fiber.

Calculations done for a taper with $A_w = 16.3 \mu\text{m}$, $L_0 = 5 \mu\text{m}$, $Z_w = 2.5 \mu\text{m}$, and $A_c = 18.3 \mu\text{m}$ also testify that the optical power is concentrated in the local modes u_{05} and u_{06} . The dependence of the total optical power P_σ on the wavelength for these modes is illustrated by curve 2 in Fig. 14. In this case, the violation of periodicity of the function $\eta(\lambda_0)$ at $\lambda_0 > 1.25 \mu\text{m}$ in Figs. 9 and 10 can be explained by lowering the power P_σ in this wavelengths range (see Fig. 14). The application of (25) to the considered taper gives $\Delta\lambda_0 = 0.048 \mu\text{m}$, which is the period that one calculates for the function $\eta(\lambda_0)$ in Fig. 9.

The tapers analyzed in this paper can be used for different sensor applications since the interference peaks can be shifted by the influence of various external parameters. Note that the propagation constants of the interfering modes depend on the refractive index and temperature of the external environment. This property was exploited for sensing the refractive index of liquids around the tapered section of an HF [10] and for sensing high temperature [24]. The length of the taper also has influence on interference fringes. Thus, minute elongation of the taper will cause a shift of the interference fringes. This property can be exploited for strain sensing [25]. The sensing of other parameters that can be translated to refractive index or strain is also possible.

The advantages of HF tapers with collapsed air holes for optical sensing are listed as follows. 1) Interferometric working mechanism. This is recognized as the most sensitive method by the sensing community. 2) The parameter being sensed is codified in an absolute parameter, the wavelength. With an optical spectrum analyzer, it is simple and straightforward to monitor the shift of the interference fringes. 3) The taper's

interference pattern is really stable and immune to drifts or fluctuations of the optical source employed. 4) The tapers operate with long-life and low-cost LEDs and can be spliced to conventional optical fibers which may reduce the overall cost of the sensors dramatically. 5) The fabrication of the tapers is simple and can be carried out in a few minutes. In addition, one can adjust the taper geometry during fabrication.

Note that similar oscillatory patterns were obtained for biconical tapers made from conventional single-mode fibers ($A_w < 5 \mu\text{m}$) [23], [26], [27]. Such tapers are more difficult to realize with long uniform beating regions (i.e., with L_0 greater than 3 mm) [23]. Tapers with such small dimensions are not easy to handle, and for some sensing applications, they are impractical.

It may be concluded that the proposed theoretical model of tapers based on large-mode-area HFAs allows the explanation of some peculiarities of their transmission. The agreement between theory and experiment is satisfactory. The presented analysis allows us to conclude that the experimentally observed oscillatory transmission spectra can be explained by interference of the modes supported by the solid taper waist. The period of the transmission function can be evaluated by the simple analytical function (25). For the studied tapers, the periodic transmission function is formed due to the interference between two local modes u_{05} and u_{06} , which concentrate most of the optical power.

REFERENCES

- [1] P. S. J. Russel, "Photonic crystal fibers," *Science*, vol. 299, no. 5605, pp. 358–362, Jan. 2003.
- [2] A. Bjarklev, J. Broeng, and A. S. Bjarklev, *Photonic Crystal Fibres*. Boston, MA: Kluwer, 2003.
- [3] T. M. Monro, W. Belardi, K. Furusawa, J. C. Bagget, N. G. R. Broderick, and D. J. Richardson, "Sensing with microstructured optical fibers," *Meas. Sci. Technol.*, vol. 12, no. 7, pp. 854–858, Jul. 2001.
- [4] J. M. Fini, "Microstructure fibres for optical sensing in gases and liquids," *Meas. Sci. Technol.*, vol. 15, no. 6, pp. 1120–1128, Jun. 2004.
- [5] S. O. Konorov, A. Zheltikov, and M. Scalora, "Photonic-crystal fiber as a multifunctional optical sensor and sample collector," *Opt. Express*, vol. 13, no. 9, pp. 3454–3459, Apr. 2005.
- [6] J. B. Jensen, P. E. Hoiby, G. Emilianov, O. Bang, L. H. Pedersen, and A. Bjarklev, "Selective detection of antibodies in microstructured polymer optical fibers," *Opt. Express*, vol. 13, no. 15, pp. 5883–5889, Jul. 2005.
- [7] T. M. Monro, D. J. Richardson, and P. J. Bennet, "Developing holey fibers for evanescent field devices," *Electron. Lett.*, vol. 35, no. 14, pp. 1188–1189, Jul. 1999.
- [8] Y. K. Lize, E. C. Magi, V. G. Ta'eed, J. A. Bolger, P. Steinvurzel, and B. J. Eggleton, "Microstructured optical fiber photonic wires with sub-wavelength core diameter," *Opt. Express*, vol. 12, no. 14, pp. 3209–3217, Jul. 2004.
- [9] E. C. Magi, H. C. Nguyen, and B. J. Eggleton, "Air-hole collapse and mode transitions in microstructured fiber photonic wires," *Opt. Express*, vol. 13, no. 2, pp. 453–459, Jan. 2005.
- [10] V. P. Minkovich, A. V. Kir'yanov, D. Monzón-Hernández, S. Calixto, A. B. Sotsky, and L. I. Sotskaya, "Holey fiber tapers with resonance transmission for high-resolution refractive index sensing," *Opt. Express*, vol. 13, no. 19, pp. 7609–7614, Sep. 2005.
- [11] V. P. Minkovich, A. V. Kir'yanov, A. B. Sotsky, and L. I. Sotskaya, "Large-mode-area holey fibers with a few air channels in cladding: Modeling and experimental investigation of modal properties," *J. Opt. Soc. Amer. B, Opt. Phys.*, vol. 21, no. 6, pp. 1161–1169, Jun. 2004.
- [12] V. P. Minkovich, A. V. Kir'yanov, and S. Calixto, "Large-hole-large-spacing holey fibers with a few air holes: Fabrication and measurements of light-delivering properties and optical losses," *Laser Phys.*, vol. 14, no. 5, pp. 767–771, May 2004.
- [13] J. Villatoro, D. Monzón-Hernández, and E. Mejia, "Fabrication and modeling of uniform-waist single-mode tapered optical fiber sensors," *Appl. Opt.*, vol. 42, no. 13, pp. 2278–2283, May 2003.
- [14] A. W. Snyder and J. D. Love, *Optical Waveguide Theory*. New York: Chapman & Hall, 1983.
- [15] N. N. Voitovich, B. Z. Katsnelbaum, A. N. Sivov, and A. D. Shatrov, "Own waves of dielectric waveguides of composite profile," *Radiotekhn. i Electron.*, vol. 24, no. 7, pp. 1245–1263, 1979.
- [16] T. M. Monro, D. J. Richardson, N. G. R. Broderick, and P. J. Bennet, "Holey optical fibers: An efficient modal model," *J. Lightw. Technol.*, vol. 17, no. 6, pp. 1093–1101, Jun. 1999.
- [17] G. Korn and T. Korn, *Mathematical Handbook*. New York: McGraw-Hill, 1968.
- [18] A. B. Sotsky and L. I. Sotskaya, "Modes of capillary optical fibers," *Opt. Commun.*, vol. 230, no. 1–3, pp. 67–79, Jan. 2004.
- [19] M. J. Steel, T. P. White, C. M. De Sterke, R. C. McPhedran, and L. C. Botten, "Symmetry and degeneracy in microstructured optical fibers," *Opt. Lett.*, vol. 26, no. 8, pp. 488–490, Apr. 2001.
- [20] H. C. Nguyen, B. T. Kuhlmev, M. J. Steel, C. L. Smith, E. C. Magi, R. C. McPhedran, and B. J. Eggleton, "Leakage of the fundamental mode in photonic crystal fiber tapers," *Opt. Lett.*, vol. 30, no. 10, pp. 1123–1125, May 2005.
- [21] M. Abramowitz and I. Stegun, *Handbook of Mathematical Functions*. Washington, DC: USA National Bureau Standards, 1964.
- [22] E. C. Magi, P. Steinvurzel, and B. J. Eggleton, "Transverse characterization of tapered photonic crystal fibers," *J. Appl. Phys.*, vol. 96, no. 7, pp. 3976–3982, Oct. 2004.
- [23] S. Lacroix, F. Gonthier, R. J. Black, and J. Bures, "Tapered-fiber interferometric wavelength response: The achromatic fringe," *Opt. Lett.*, vol. 13, no. 5, pp. 395–397, May 1988.
- [24] D. Monzón-Hernández, V. P. Minkovich, and J. Villatoro, "High-temperature sensing with tapers made of microstructured optical fibers," *IEEE Photon. Technol. Lett.*, vol. 18, no. 3, pp. 511–513, Feb. 2006.
- [25] J. Villatoro, V. P. Minkovich, and D. Monzón-Hernández, "Temperature-independent strain sensor made of tapered holey optical fiber," *Opt. Lett.*, vol. 31, no. 3, pp. 305–307, Feb. 2006.
- [26] S. Lacroix, R. J. Black, C. Veilleux, and J. Lapierre, "Tapered single-mode fibers: External refractive-index dependence," *Appl. Opt.*, vol. 25, no. 15, pp. 2468–2469, Aug. 1986.
- [27] D. T. Cassidy, D. C. Johnson, and K. O. Hill, "Wavelength-dependent transmission of monomode optical fiber tapers," *Appl. Opt.*, vol. 24, no. 7, pp. 945–950, Apr. 1985.



Vladimir P. Minkovich (M'04) received the M.Sc. degree in chemical engineering and technology from the Belarussian Technological Institute (the University since 2000), Minsk, Belarus, in 1973, and the Ph.D. degree in optical systems of location, communication, and information processing from the Institute of Electronics, National Academy of Sciences of Belarus, Minsk, in 1986.

He has worked on problems of optical fiber technology since 1975 as a Researcher with the Institute of Applied Optics of the National Academy of Sciences of Belarus, Mogilev, Belarus, and with the Institute of Radio Engineering and Electronics (IRE), Russian Academy of Sciences, Fryazino, Moscow Region, Russia. Since 1999, he has been with the Centro de Investigaciones en Óptica, A.C., Leon, Mexico, as a Research Scientist. He is the author or coauthor of nearly 30 scientific publications. He is the holder of ten patents, and with another three in procedure. His current research interests include design, development, fabrication, and investigation of special conventional and microstructured optical fibers for communication, fiber lasers, and sensor applications.

Dr. Minkovich is a member of the Optical Society of America and the International Society for Optical Engineering (SPIE).

David Monzón-Hernández (M'05) received the B.Eng. degree in communications and electronics from the University of Guanajuato, Guanajuato, Mexico, in 1993, and the M.Sc. and Ph.D. degrees in optics from the Centro de Investigaciones en Óptica, A.C., Leon, Mexico, in 1995 and 1999, respectively.

In 2000, he joined the Department of Applied Physics, University of Valencia, Valencia, Spain, as a Postdoctoral Fellow. Since March 2002, he has been a Research Associate with the Department of Fiber Optics, Centro de Investigaciones en Óptica, A.C. His main research interests are optical sensors based on fiber Bragg gratings and evanescent field interactions.

Dr. Monzón-Hernández is a member of the International Society for Optical Engineering (SPIE).



Joel Villatoro (M'06) received the B.Sc. degree in physics from the Autonomous University of Puebla, Puebla, Mexico, in 1992, and the M.Sc. and Ph.D. degrees in optics from the National Institute for Astrophysics, Optics, and Electronics, Puebla, in 1995 and 1999, respectively.

He was a Visiting Scholar for two-and-a-half years at the Centro de Instrumentos, National Autonomous University of Mexico, Mexico City. In 1999, he joined the Case Western Reserve University, Cleveland, OH, as a Research Associate. One year

later, he joined the University of Valencia, Valencia, Spain, as a Postdoctoral Fellow. From November 2001 to November 2005, he worked as a Research Scientist with the Centro de Investigaciones en Optica A.C., Leon, Mexico. Since January 2006, he has been a "Ramón y Cajal" Researcher with the Nanophotonics Group, Institute of Photonic Sciences, Castelldefels, Barcelona, Spain. He is the author or coauthor of nearly 40 scientific publications. He has two patents in procedure. He has been a Reviewer of several papers submitted to different journals. His main research interests are the fabrication of sensors and devices based on conventional and microstructured optical fibers and on the excitation of localized or hybrid surface plasmons.

Mr. Villatoro is a Regular member of the IEEE Lasers and Electro-Optics Society and the Optical Society of America.



Alexander B. Sotsky received the M.S. degree in physics from the Belarussian State University, Minsk, Belarus, in 1976 and the Ph.D. and D.Sc. degrees in optics from the Institute of Physics, National Academy of Sciences of Belarus, Minsk, in 1983 and 2002, respectively.

He is a Professor with the Department of Experimental and Theoretical Physics, Mogilev State University, Mogilev, Belarus. His current research interests include inverse optical problems, scatterometry, design, and mathematical modeling of waveguide and fiber-optic sensors.



Luidmila I. Sotskaya received the M.S. degree in physics from the Mogilev State University, Mogilev, Belarus, in 1976 and the Ph.D. degree in optics from the Gomel State University, Gomel, Belarus, in 2005.

She is a Reader with the Department of Mathematics, Mogilev State Foodstuffs University, Mogilev, Belarus. Her current research interests include mathematical modeling of integrated and fiber-optic devices.